IEEE Open Journal of Engineering in Medicine and Biology

Technology

Multiscale Model Development for Electrical Properties of Thyroid and Parathyroid Tissues

M. Matella, K. Hunter, S. Balasubramanian, *D. C. Walker

***Abstract*—*Goal:* Electrical impedance spectroscopy (EIS) has been suggested as a possible technique to differentiate between thyroid and parathyroid tissue during surgery. This study aims to explore this potential using computational models to simulate the impedance spectra of these tissues, and examine how they are influenced by specific differences in tissue composition and morphology. *Materials and methods:* Finite element models of thyroid and parathyroid tissues at multiple scales were created, and simulated spectra were compared to existing data collected using ZedScan^{TM} probe during surgery. Geometrical and material properties were varied in a local sensitivity study to assess their relative influence. *Results:* Both simulated and measured EIS parathyroid spectra show a higher β dispersion frequency relative to thyroid. However, impedances exhibit overlap at frequencies below 100 kHz. A computational sensitivity study identified uncertainties in extracellular space dimensions, and properties of colloid and fascia compartments as having a significant effect on simulated impedance spectra characteristics. *Conclusions:* We have demonstrated the utility of our multiscale model in simulating impedance spectra and providing insight into their sensitivity to variations in tissue features. Our results suggest that distinguishing between the thyroid and parathyroid spectra is challenging, but could be improved by constraining the properties of colloid and fascia through further computational or experimental research.**

***Index Terms*—Electrical Impedance Spectroscopy, Finite Element Modelling, Thyroid and Parathyroid Tissue Discrimination, Thyroidectomy**

***Impact Statement*- The presented computational study investigated the electrical impedance spectroscopy as a potential method to discriminate thyroid and parathyroid tissue during thyroidectomy.**

I. INTRODUCTION

THYROIDECTOMY is a well-established surgical procedure that encompasses various types of thyroid surgeries. The most prevalent complications associated with the procedure are hypoparathyroidism and hypocalcaemia that are both a result of inadvertent damage or excision of the adjacent parathyroid glands. According to the UK Registry of Endocrine and Thyroid Surgeons which is the most coherent documentation of thyroidectomies performed between 2010-2014 in the UK, 23.6 and 6.5% of patients having whole gland thyroidectomy, respectively, experienced temporary or late hypocalcaemia [1].

The major concern during the surgery are the parathyroid glands themselves, which, due to their small size and location, could be mistaken for other structures (adipose tissues, lymph nodes or benign thyroid nodules) [2]. In general, surgeons rely on their own experience and judgement during the surgery to locate and preserve normal parathyroid glands. However, introducing an additional measurement tool that would guide the surgeon during the procedure, would be beneficial to decrease the risks of hypoparathyroidism and hypocalcaema. To date, fluorescence imaging has been considered a potentially useful aid to the surgeon to differentiate parathyroid glands from adjacent tissues [3], [4].

A. Electrical Impedance Spectroscopy

Electrical Impedance Spectroscopy (EIS) is a measurement technique that could be incorporated to the thyroidectomy procedure. In its principle, a small alternating current is passed through soft tissues, and the resultant impedance is measured across a range of frequencies, allowing the construction of a characteristic impedance curve, or "spectrum" for that tissue. The diagnostic value of EIS has been documented and implemented to detect lesions in skin [5], cervix [6], oral tissue [7], bladder [8], prostate [9], breast tissue [10] and oesophagus [11]. After being exposed to electrical field, the electrical conduction by the biological structures is possible due to the ions concentrated in different structures. Moreover, tissues are capable not only of conducting, but also of retaining electrical charge, which is attributed mainly to the properties of the cell membranes. In the case of biological tissues, EIS spectra are characterised by the β dispersion – a substantial fall in the real part of impedance values in the kHz-MHz region, which is a result of the capacitive nature of the cell membrane.

The principle of measurement of a typical tetrapolar EIS device is shown in Fig. 1 with the example of a commercial probe ZedScan^{TM}, Zilico Limited, currently licensed for use to detect changes in cervical epithelium accompanying colposcopy. A known magnitude of the alternating current I flows through the two active electrodes, meanwhile, passive electrodes capture the potential difference required to the impedance calculation at each frequency.

Furthermore, the electrical behaviour of biological tissues has been a subject of various computational studies documented in the literature. Multiscale Finite Element (FE) models

This paper got submitted for review on June 26th, 2023.

M. Matella and *D. C. Walker are with the Computer Science Department, University of Sheffield, Sheffield S1 4DP, UK and Insigneo, Institute for in silico Medicine, Sheffield S1 3JD, UK (correspondence e-mail: d.c.walker@sheffield.ac.uk).

K. Hunter is with the Liverpool Head and Neck Centre, Molecular and Clinical Cancer Medicine, University of Liverpool, Liverpool L69 7TX, UK

S. Balasubramanian is with Department of Oncology and Metabolism, Royal Hallamshire Hospital School of Medicine and Biomedical Sciences, University of Sheffield, Sheffield S10 2RX, UK

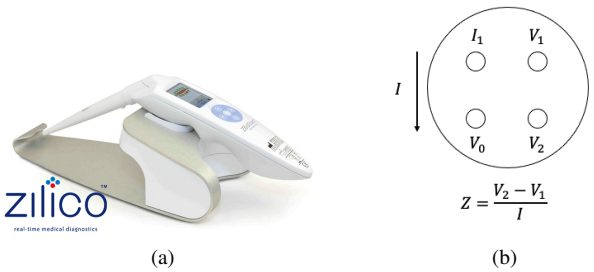

(a) (b)

Fig. 1. Electrical Impedance Spectroscopy device: (a) ZedScan™ [12], (b) tip of the tetrapolar probe showing the principle of the measurement, a known current I flows between the active electrodes (I_1 and V_0) while the passive electrodes (V_1 and V_2) capture the potential difference at each frequency

relating to the EIS tetrapolar probe measurements of cervical epithelium [13], bladder [14] and oral tissues [15] have been developed to determine the changes in tissues electrical properties due to cancerous lesions. Some studies have focused on skin, such as a FE model simulating the electrical properties of skin pathologies [16], or assessing the thickness of stratum corneum with an analytical model [17]. Another research group proposed a parameterisation method to investigate the impact of the cell shapes on their electrical properties [18] and expanded the research to skin properties investigation using analytical and numerical methods [19]. There is only one study [20] constructing a FE model to explore the electrical and heat transfer properties of thyroid tissue, with the emphasis on the follicular structure and colloid's conductivity. Nonetheless, the cellular details have not been included in this model nor studied separately in this case.

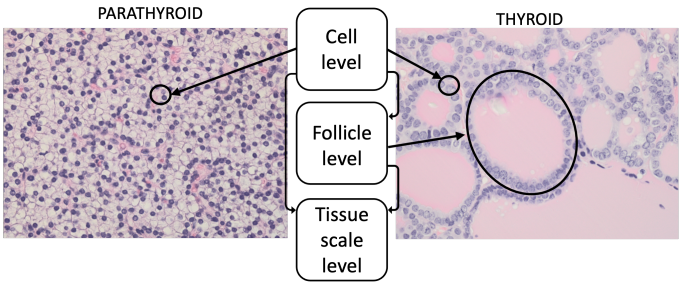

Fig. 2. Thyroid and parathyroid histology images with labelled levels of complexity corresponding to the levels of the computational model

B. Aim of the study

The differences in the thyroid and parathyroid impedance recorded with an EIS probe have already been evaluated empirically in [2] suggesting the regions in both tissues' spectra that could allow their discrimination. However, the EIS measurements solely inform of the bulk electrical properties without the ability to make the connection between the recorded impedance spectra and the tissue characteristics responsible for the observed behaviour. That connection, however, can be explored by implementing computational modelling to accompany the EIS experimental results and complement them in order to provide more insight into the mechanisms that influence tissue impedance.

Moreover, as previous research has demonstrated [6], [13], the frequency-dependent impedance, and hence the shape of the dispersion, depend on the geometrical characteristics and organisation of the structures within the tissue, along with the tissues' material composition and their electrical properties. Therefore, tissue types' structural differences at the cellular or supra-cellular level might be expected to give rise to different impedance curves. Those differences in the case of thyroid and parathyroid tissue (Fig.2) are substantial with thyroid being composed of an arrangement of cell-lined colloid-filled follicles, which are entirely absent in parathyroid, the latter being composed of closely packed chief cells.

The aim of this project is to develop a mechanistic model recreating thyroid and parathyroid tissues' structure and composition, to simulate their theoretical electrical behaviour and to compare against the in vivo measurements presented in [2]. Furthermore, the influence of specific features of thyroid and parathyroid tissue structure on different characteristics of the impedance spectra will be investigated through a local sensitivity study.

II. MATERIALS AND METHODS

A. Finite element modelling of electrical tissue properties

As highlighted in the Introduction, computational models can be a useful tool to simulate and evaluate the effect of various tissue characteristics on the impedance spectra. For the purposes of this study, numerical modelling (of which the FE approach is an example) is more suitable than the analytical methods, such as Maxwell Mixture Theory [21], that requires numerous assumptions in the structure of the model and its homogeneity which are not adequate in the context of thyroid and parathyroid. FE analysis is a well-established numerical method for solving electric field problems, including in biological systems. Through the process of discretisation, boundary conditions and assignment of element material properties, FE modelling can approximate the potential distribution within the domain. The latter is divided into a substantial number of small elements connected at nodes where the electric scalar potential is being approximated based on the assigned boundary conditions and material properties, such as electric conductivity and relative permittivity in the case of an electrical simulation. For this study, the quasistatic time-harmonic simulation approach has been applied using the FE commercial software Ansys Mechanical APDL. Further details concerning the electrical scalar potential approximation are summarised in the Supplementary Materials Section I.

B. Multiscale model development

As previously mentioned, the unique frequency-dependent properties of tissues are a result of the capacitive nature of cell membranes, which makes them a crucial component for inclusion in the model. However, due to their small size (~8 nm), it is not computationally feasible to include them in a tissue model recreating the impedance measurement with EIS

probe, which requires a simulation volume of the order of centimetres. Such a model would comprise over trillion nodes for thyroid tissue only, which is computationally intractable.

To overcome this limitation, a multiscale modelling approach was implemented, where the tissue's structure is considered as a set of hierarchical substructures, representing different levels of complexity from cellular level (microscale) to tissue level (macroscale). For the thyroid tissue, an additional scale (mesoscale) has been included to reconstruct this tissue's basic structural unit – the follicle. The models of different scale are visualised in Fig. 3.

Transfer impedivities are calculated, starting with the lowest model hierarchy (microscale) and passed to the higher level models in the form of element material properties. For lower scale models (cell and follicle), the effective impedivity is simulated at 14 frequency points f from the range of 76Hz – 625kHz which correspond to the measurement points and range of the Zedscan^{TM} device. Subsequently, the results are processed to calculate electric conductivity (σ) and relative permittivity (ε_r) from (1) and (2), to assign as material properties in the appropriate higher-level model compartments:

$$\sigma(f) = d/(A \cdot Z'(f)) \tag{1}$$

$$\varepsilon_r(f) = (Y''(f)/2\pi f \cdot \varepsilon_0) \cdot (d/A) \tag{2}$$

where:

$$Y''(f) = -Z''(f)/((Z'(f))^2 + (Z''(f))^2) \tag{3}$$

where:

where: d and A – thickness and cross-sectional area of the model, ε_0 – permittivity of free space (8.854 x 10^{-12} Fm^{-1}), Z' and Z'' – real and imaginary part of effective impedance obtained from lower level simulation, Y'' – imaginary part of admittance. The derived electrical material properties are then transferred to the appropriate elements of the adjacent higher scale model, according to the tissues' hierarchical structure, i.e. thyroid microscale level results are assigned to the cell layer compartment elements of the mesoscale model, and then the follicle mesoscale results are passed on to the thyroid compartment at macroscale. Similarly, the parathyroid microscale results are assigned to elements of this gland's compartment at the macroscale level (as there is no mesoscale model for parathyroid tissue).

Thyroid model:

The microscale model (Fig. 3a) consists of three compartments: cytoplasm, cell membrane and extracellular space (ECS) layer. All simulated cells are anuclear due to the outcomes of previous research [13] which concluded that due to the more conductive properties of the nuclear membrane in comparison to the cell membrane, the nucleus and its membrane have a negligible effect on the effective electrical properties of cells. The mesoscale model (Fig. 3b) comprises colloid (a protein-rich material), homogenised cells (material properties obtained from the microscale level simulation) and connective tissue layer compartments. All models assume simplified cuboidal structures after initial exploration demonstrated that shape and arrangement have a negligible effect on impedance properties compared to other characteristics of interest (data not shown).

The macroscale model recreates the electrode arrangements of a tetrapolar EIS ZedScan^{TM} probe with the 0.6 µm electrodes arranged with the centers located on a circle of 2 mm diameter (Fig. 3e). The impedance is obtained by dividing the injected current of 6 µA assigned to the driving electrode (I_1) by the potential difference recorded by the passive electrodes (V_1 and V_2). The dimensions of the macroscale models were identical for both tissue types: 40x40x15 mm (the cross-section through the cuboid thyroid model is shown in Fig. 3c). A superficial fascia layer was included in this model, representing loose connective tissue which encapsulates the glands. The surgeon is able to distinguish and peel off the superficial fascia before placing the probe for the EIS measurement, however, the extent of tissue removal cannot be guaranteed. Hence the effects of fascia layer, its thickness and material properties are also explored in this study.

Parathyroid model:

Reflecting on the parathyroid's tight cellular morphology, only two sublevels in multiscale modelling have been recognised. The microscale parathyroid model was constructed in the same manner as the three-compartmental thyroid cell model (Fig. 3a). Moreover, the parathyroid macroscale model shows similarities to the thyroid model in terms of dimensions and the boundary conditions set up. The model adjusted to the parathyroid recreates the tissue layout when the EIS measurement is performed when parathyroid is surrounded by thyroid tissue - on the posterior surface of the thyroid - and the electrodes are positioned symmetrically in the centre of the gland (Fig. 3d).

C. Parameter sensitivity study

To investigate the impact of various geometrical and electrical properties of the compartments in all submodels on the macroscale impedance, a local intercompartmental sensitivity analysis was performed in an one-at-a-time (OAT) manner to determine the isolated effects of the parameters on the simulation results. In the intercompartmental analysis, the studied input parameters belong to structures across different scales and their effects are propagated and evaluated at the highest scale, in this case by comparing the macroscale computed EIS spectra. For each parameter, its baseline (usually mean of values reported in the literature), minimum and maximum values have been chosen for analysis (in a few cases, more than three points have been selected to better cover the whole parameter range), with remaining parameters fixed to their baseline value. The parameters' range has been decided based on the values documented in the literature and our own histology measurements.

There have been thirteen input parameters investigated for thyroid tissue (seven relating to morphological characteristics and six to electrical properties uncertainties), and eight for parathyroid (six geometrical, two electrical). In previous work [13] in electrical properties of cells, the effects of the uncertainties in the material properties of the cell compartments have been investigated, hence, were excluded from this study and kept constant throughout all simulations along with the cell membrane thickness (8 nm).

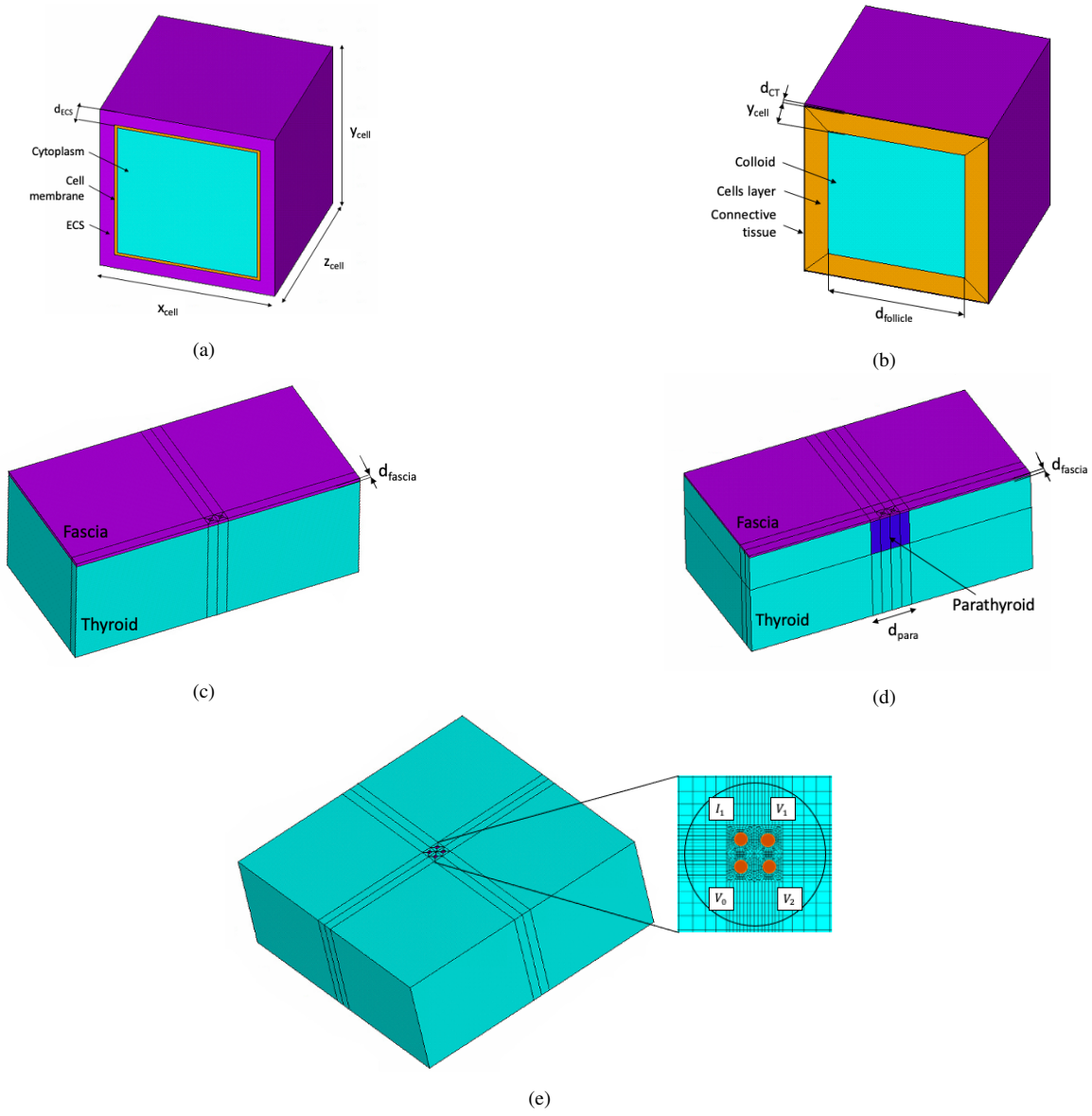

Fig. 3. Multiscale model developments with labeled compartments: (a) microscale model, (b) mesoscale model, (c) thyroid macroscale model, (d) parathyroid macroscale model, (e) macroscale model with the electrode pattern, where: x_{cell}, y_{cell}, z_{cell} - cell dimensions, d_{ECS} - ECS thickness, $d_{follicle}$ - dimensions of colloid compartment in the mesoscale model , d_{CT} - connective tissue thickness, d_{fascia} - fascia thickness, d_{para} - dimensions of parathyroid gland, (I_1 and V_0) - active electrodes, (V_1 and V_2) - passive electrodes

Full list of the values of the investigated and fixed parameters is summarised in detail in Section II of Supplementary Materials (Tables II and III) with further discussion.

D. Parametrisation of simulated spectra

In order to make a quantitative comparison between the results, each simulated spectrum has been parameterised by selecting three indices: two impedance values Z_1 and Z_{14} at the lowest and highest frequency points (76 Hz and 625 kHz), and the dispersion frequency f_{mid} at the centre of the dispersion (frequency for when impedance takes the mid-point value between Z_1 and Z_{14}).

E. Comparison with in vivo measurements

The in vivo measurements were previously published [2] and the experimental data from the thyroid and parathyroid tissue was used in the study with the authors' permission. The mean EIS measurements of thyroid (n=53) and parathyroid (n=42) have been taken for the analysis and, similarly to the simulated spectra, three indices, Z_1, Z_{14} and f_{mid} extracted for each experimental spectrum for the quantitative comparison.

III. RESULTS

All computed results presented are real impedance values at 14 frequencies in the range between 76Hz-625kHz from the macroscale model simulations (the lower-scale results in a form of electrical material properties are summarised in

the Supplementary Dataset). The study resulted in 36 and 19 computed EIS spectra, where each of the input parameters was investigated in the OAT sensitivity study for thyroid and parathyroid respectively. To aid the quantitative comparison, the Z_1, Z_{14} and f_{mid} spectra indices have been derived for each computed and measured in vivo spectrum.

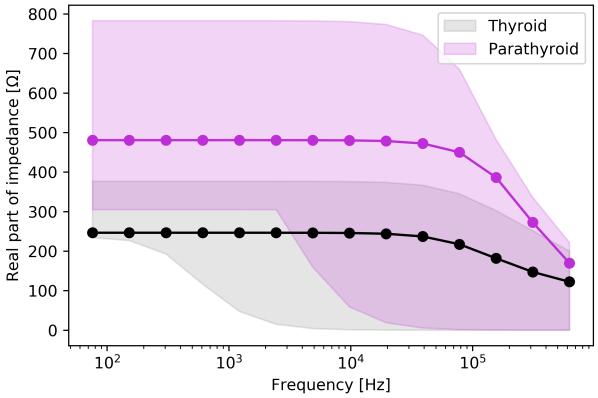

Fig. 4. Baseline computed impedance spectra obtained with the default input parameters for thyroid (black spectrum) and parathyroid (pink spectrum) tissues with marked range of all computed results obtained through the variation of geometrical and electrical properties summaries in Table II and III from Supplementary Materials

A. Computed impedance spectra

The frequency-dependent baseline impedance spectra obtained for thyroid and parathyroid tissues with the range of the curves generated by varying geometrical and electrical properties (summarised in Table II and III from Supplementary Materials) are displayed in Fig. 4. These results imply that it is expected to observe higher impedance across all frequencies for the parathyroid compared to thyroid when both models are at their default configuration of morphological and electrical properties. However, the inspection of the results' range reveals an overlap between the computed results that increases with the frequency.

B. Computed and measured in vivo impedance comparison

Computed spectra are plotted against the range of the experimental results in Fig. 5. The presentation of individual simulated spectra rather than simply the baseline curve (as shown in Fig. 4) permits the inspection of the variation in the shape of individual spectra according to the investigated variation in the morphology and electrical properties. It is apparent that there are similarities with in vivo measurements observed for both thyroid and parathyroid tissues. However, at frequencies below 100kHz, the computed thyroid spectra correspond to the lower impedance values from the experimental data, with the opposite trend for the parathyroid case.

The quantitative comparison of the mean (±standard deviation) values of extracted spectra parameters (Z_1, Z_{14} and f_{mid}) is presented in Table I. A visual comparison of the experimental and computational chosen spectra parameters is pictured in Fig. 6. Similar trends of higher mean Z_{14} and f_{mid} for parathyroid tissue is documented for both computed and experimental results as seen in Table I and Fig. 6b and 6c. Conversely, the Z_1 computed results did not predict higher values for thyroid tissue over the parathyroid as observed in the experimental data. Nonetheless, the visual comparison of the spectra indices highlights that the majority of the computed results is in agreement and within the range of the experimental data.

SELECTED SPECTRA INDICES

	Thyroid	Parathyroid
Computed:		
$Z_1[\Omega]$	239.02 (±40.26)	464.92 (±114.95)
$Z_{14}[\Omega]$	103.58 (±50.43)	120.06 (±66.31)
$f_{mid}[kHz]$	139.86 (±62.26)	192.00 (±79.48)
Experimental:		
$Z_1[\Omega]$	325.42 (±117.00)	280.58 (±97.37)
$Z_{14}[\Omega]$	112.50 (±15.67)	132.70 (±35.50)
$f_{mid}[kHz]$	62.23 (±48.52)	157.26 (±69.67)

TABLE I. The mean (±standard deviation) values for the extracted spectra indices for the computed and experimental results for both tissue types.

C. Parameter sensitivity study

Finally, an itercompartmental local sensitivity study has been performed to investigate the isolated effect of each morphological and electrical input parameter on the selected macroscale spectra indices: Z_1, Z_{14} and f_{mid}. The parameters were varied accordingly to the values presented in Section II of Supplementary Materials (Tables II and III) in the OAT manner. Each bar shows the maximum and minimum percentage change from the mean result calculated for each parameter.

Thyroid: geometrical parameters

As shown in Fig. 7a, thyroid impedance results were predominantly sensitive to changes in the size of the follicles ($d_{follicle}$) at the low frequencies (Z_1) and the thickness of the connective tissue (d_{ct}) at high frequencies (Z_{14}). The greatest differences in the middle frequency (f_{mid}) results were observed for the variations in the ECS thickness (d_{ECS}). All three extracted indices were insensitive to the changes in the cell width - dimension in the z direction (z_{cell}).

Thyroid: material properties

Fig. 7b shows the results for the sensitivity analysis of the material properties of the thyroid model compartments. Among the parameters studied, the colloid conductivity ($\sigma_{colloid}$), connective tissue and fascia relative permittivity (εr_{CT} and εr_{fascia}) are those that have the most substantial impact on all three indices, while variation in the other parameters resulted in less than $\pm 25\%$ variation from the mean value of the spectra parameters.

Parathyroid parameter study

Fig. 7c shows that the ECS thickness (d_{ECS}) and cell length - size in the x direction (x_{cell}) - have the most significant influence on the Z_1. Similarly to the results from the thyroid model, the high frequency impedance is more sensitive to the changes in fascia thickness (d_{fascia}) and its permittivity

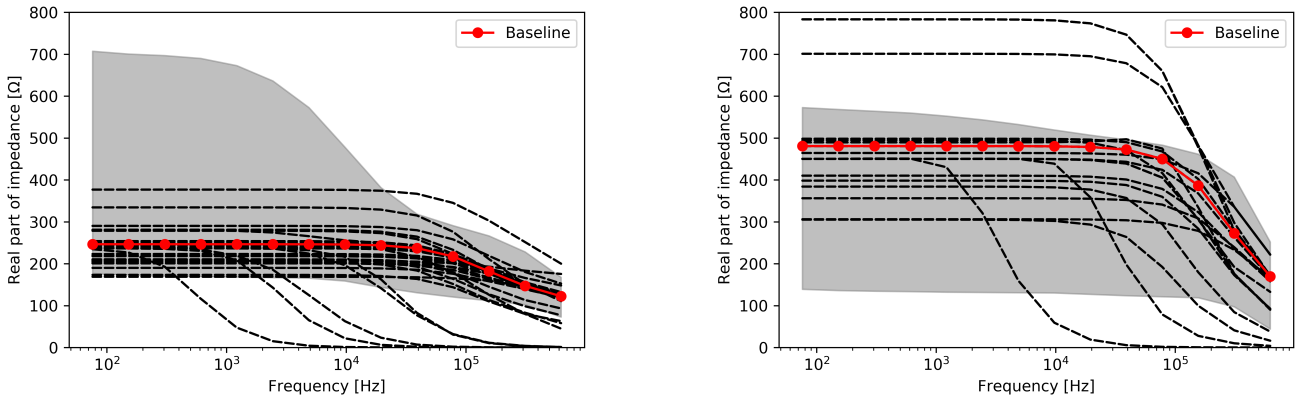

(a) (b)

Fig. 5. Comparison of the computed spectra (black dashed lines, with the red dotted line marking the baseline spectrum) against the range of experimental data (grey range) for: (a) thyroid, (b) parathyroid tissue

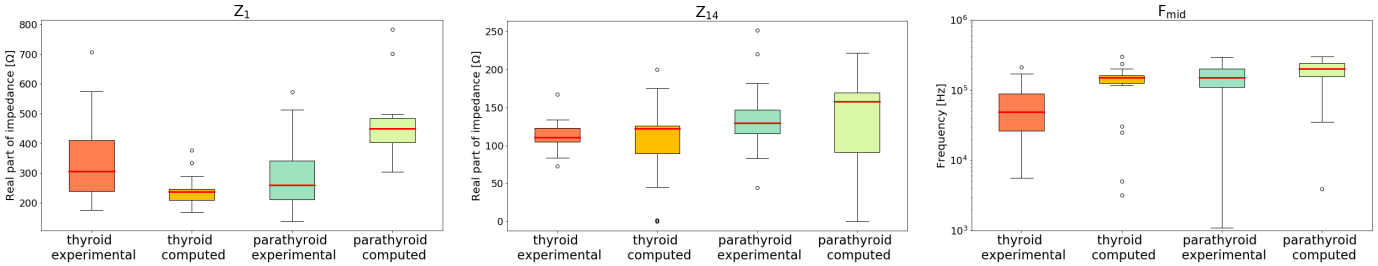

(a) (b) (c)

Fig. 6. Box and whisker plot of the extracted spectra indices (Z_1 - impedance at 76 Hz, Z_{14} - impedance at 625kHz and f_{mid} - dispersion frequency) comparing both glands and the computed and experimental results

(εr_{fascia}), with the middle frequency also exhibiting sensitivity to the latter (εr_{fascia}).

IV. DISCUSSION

The purpose of this study was to develop and apply a computational model to investigate the potential of electrical impedance spectroscopy to differentiate tissues during thyroidectomy. The presented multiscale finite-element modelling pipeline was designed to simulate the theoretical EIS spectra for thyroid and parathyroid tissues in order to analyse and compare them to curves obtained during in vivo measurements. Moreover, the effects of the variability in geometrical parameters and uncertainty in material properties of these tissues at micro-, meso- and macroscales on the ”measured” impedance have been evaluated.

A qualitative comparison of simulated results, as shown in Fig. 4, indicates a distinct difference between the baseline thyroid and parathyroid spectra. The baseline results suggest the parathyroid impedance is expected to be higher than thyroid impedance, with the parathyroid impedance value being about 95% and 37% higher than for the thyroid at 76Hz and 625kHz respectively. However, it is worth noting that there is an overlap in the whole range of computed spectra resulting from various input parameters investigation. Nonetheless, as seen in Fig. 5 most of the theoretical curves are in close proximity to the baseline result of both glands. A few outliers characterised with low-frequency β dispersion that are affecting the low range of results are the outcome of the examination of varying connective tissue and fascia permittivities, and do not represent the trend of the remaining computed results. The high values of permittivity (over 1e6) assigned in those instances correspond to the values reported for the tendon, which, despite its high collagen composition, is characterised with a different structure compared to fascia or thyroid connective tissue and thus such values can be excluded from future simulations.

The comparison between the simulated and in vivo results from Fig. 5 shows that the majority of the theoretical spectra predicted by our model lies within the range of the experimental EIS curves. The best fit can be observed in the frequency region above 100kHz for both tissue types. However, a closer inspection of the spectra indices presented in Fig. 6a and Table I, reveals discrepancies between the computed and in vivo results in the Z_1 index representing the low-frequency impedance. In contrast to the differences in computed results seen in in Fig. 4, the experimental data reports the opposite tendency, with higher low-frequency values for thyroid compared to parathyroid. Fig. 5 and 6 show wide variation in both modelled and measured data, which will contribute to this discrepancy.

It is important to note that the baseline results (red curves

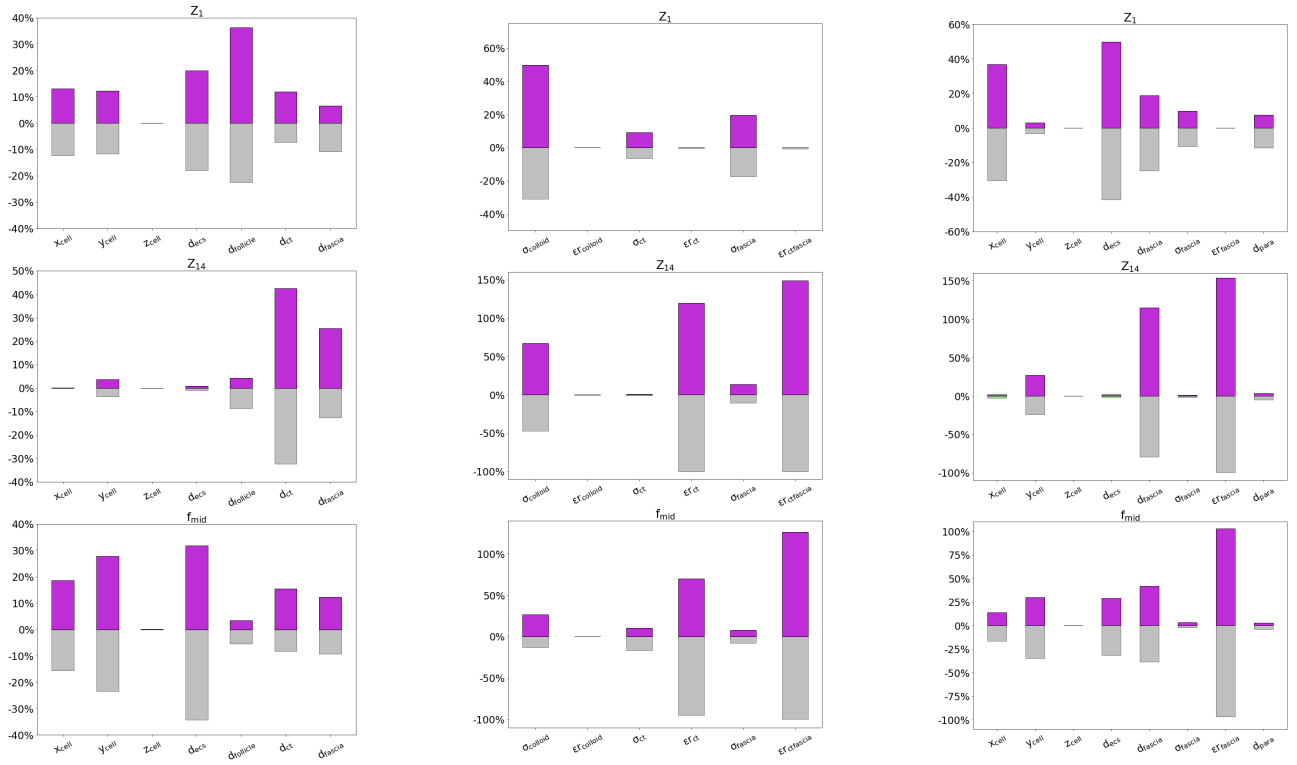

(a) (b) (c)

Fig. 7. Parameter sensitivity analysis results: (a) thyroid geometrical parameters, (b) thyroid material properties, (c) parathyroid parameters; x_{cell}, y_{cell}, z_{cell} - cell dimensions, d_{ECS} - ECS thickness, $d_{follicle}$ - dimensions of colloid compartment in the mesoscale model, d_{CT} - connective tissue thickness, d_{fascia} - fascia thickness, d_{para} - dimensions of parathyroid, $\sigma_{colloid}$ - conductivity of colloid, $\varepsilon r_{colloid}$ - relative permittivity of colloid, σ_{ct} - conductivity of connective tissue, εr_{ct} - relative permittivity of connective tissue, σ_{fascia} - conductivity of fascia, εr_{fascia} - relative permittivity of fascia

in 5) were generated without any attempt to adjust parameters to "fit" the measured data, which suggests the validity of a multiscale modelling approach and at least the approximate range of the morphological and electrical parameters selected. A useful feature of this computational model is the ability to explore how variations or uncertainties in either morphological features included in the model, or estimated electrical properties associated with features on different scales can impact the simulated results. In particular, our multiscale approach allows us to calculate the intercompartmental sensitivity of selected model outputs (in this case the extracted spectra indices) at the macroscale to changes in the inputs at lower scales.

As demonstrated by this sensitivity analysis, the variation in morphological parameters relating to tissue structure, as well as in the uncertainty in the electrical properties of different tissue compartments, are significant factors influencing the theoretical EIS curves. Therefore, the limitation in obtaining reliable model parameters for the model could partially explain the observed discrepancies in low-frequencies. Model cell and follicle sizes have been determined based on the values reported in the literature and our own measurements, however, other morphological parameters were not investigated as thoroughly and their magnitudes were estimated for this study purposes (e.g. ECS thickness has been determined based on previous cervical epithelium cells simulations [13] and electron emission microscopy images of dromedary camel parathyroid gland found in the literature [22]). As shown in Fig. 7a and 7c, the ECS thickness is one of the most important parameters that influences the low-frequency impedance for both tissue types, which is in agreement with previous computational studies in EIS modelling of cervical epithelium [13]. Additionally, the parameter study presented here mostly explored the effect of the extremities of the values reported in the literature which very coarsely covers the parameters' range.

The discrepancies in the simulated and in vivo measured low-frequency impedance could possibly also be explained by the measurement uncertainties associated with the experimental data collection. The surgeon separates the superficial fascia from the glands before taking the EIS measurement, however, sometimes the removal may be incomplete and it is not possible to quantify how much fascia is present on the tissue during the measurement. As demonstrated by our computational sensitivity study, all three spectra indices are sensitive to the fascia thickness and its electrical properties, with variation in fascia parameters associated with up to 150% change in impedance and dispersion frequency, notably decreasing the feasibility of tissue differentiation.

As noted in [2], the substantial variation of in vivo results could be explained by the differences in the measurements' conditions (temperature, humidity) and in the glands vascularity and viability (which is also difficult to assess during or after the surgery). Furthermore, in [2] it is discussed that the

tip of the probe of the ZedScan^{TM} device (5.5 mm) initially manufactured for the applications for cervical epithelium, is relatively large in comparison to parathyroid glands (typically 3-7 mm). Imprecise coverage of the parathyroid gland with the probe could lead to "contamination" of measurements by adjacent tissues – thyroid, fascia or adipose tissue – which is impossible to verify after the measurement. Additional computational work on probe optimisation and various probe-tissue misplacement scenarios could help to better grasp the importance of precision in EIS in vivo measurements.

In contrast to the discrepancies in the low-frequency impedance, both Z_{14} and f_{mid} indices show a similar trend for both computed and experimental results (Table I): i.e. both indices are higher for the parathyroid than thyroid tissue in simulated and measured data. Nonetheless, when the magnitude of the differences (less than 10%) and the standard deviation are taken into consideration, there is a large overlap in the range of both parameters, preventing a clear separation of thyroid and parathyroid.

Lastly, the computational model over-predicts the f_{mid} parameter for both tissue types. The reason for this could be inappropriate selection of the poorly defined fascia and connective tissue relative permittivity, since those parameters mostly influence f_{mid}, as much as the ECS thickness (Fig. 7b and 7c). An additional explanation could be in the invalid assumption of the homogeneous structure for the models, which, as discussed in [23], can result in a sharp and narrow theoretical dispersion, compared to the results obtained experimentally. As explained further, the heterogeneity in the structures of the biological material is suspected to be responsible for wider β dispersion, possibly moving the f_{mid} towards lower frequencies. This could be verified through e.g. a larger multifollicular mesoscale model representing the thyroid follicles of different shapes and sizes.

The OAT local sensitivity analysis approach is a blunt tool for assessing parameter sensitivity, with more sophisticated global parameter sensitivity analyses being the gold standard [24], especially for non-linear models. However, given the long computational runtimes of our model (up to 5 min per frequency for the parathyroid macroscale model, giving $>$ 1h of computational time to obtain each impedance curve), the OAT method provides a convenient screening tool of the effect of individual parameters within a reasonable range and, despite covering only a fraction of the parameter space, has already highlighted significant and non-significant parameters for both tissues. In particular, all three spectra indices are insensitive to variations in the input parameters: cell size in the z direction (z_{cell}) and relative permittivity of colloid ($\varepsilon r_{colloid}$), hence, those parameters can be excluded from future parameter sensitivity investigation. On the other hand, the lack of documented electrical properties of colloid, connective tissue and fascia remains a significant challenge since, as visualised in the Fig. 7b and 7c, uncertainties in those parameters are responsible for over ±100% variation from the mean values in the investigated spectra indices. Nonetheless, the outcomes of this sensitivity study will allow to narrow down the range of the parameters, such as the fascia permittivity, in the future work. In addition, a future global sensitivity analysis, where multiple input parameter values are varied simultaneously, with suitable sampling of the entire parameter space will provide a more accurate assessment of the effect of model parameter uncertainty, estimate the sensitivity of the model to the input parameters and verify the outcomes of this local sensitivity study.

Further sensitivity analysis will also provide a larger sample size of theoretical impedance spectra which could provide additional input in elucidating the features differentiating the thyroid and parathyroid, which was not possible to determine based on the results of the local sensitivity study presented in this paper. Establishing clear differences in the electrical behaviour of the two tissue types would provide the justification for incorporating the EIS measurements as a tool for tissue differentiation during thyroidectomy.

V. CONCLUSION

In this study, multiscale finite element models of thyroid and parathyroid tissues have been developed to investigate their electrical properties and simulate their theoretical impedance curves corresponding to the EIS measurement. The presented macroscale impedance results are within the range of the in vivo measured spectra. However, observed discrepancies between computed and in vivo results and similarities in studied spectra indices for both tissues suggest that differentiation of the two tissues based on their measured electrical impedance in the range studied is not straightforward. Our computational parameter sensitivity study elucidated the isolated effect of chosen input parameters on features of the impedance spectra, highlighting in particular, the significance of the variations in the geometrical parameters (ECS thickness, follicle size, connective tissue thickness) resulting from the natural inter- and intrasubject morphological variability and uncertainties in material properties (colloid conductivity, relative permittivity of connective tissue and fascia) that come from insufficient experimental data on electrical properties of biological materials.

Our study emphasises the utility of computational models as a complement to in vivo EIS data measurement, particularly as a tool to study the influence of multiscale tissue features on macroscopic electrical properties. Further work will include a global sensitivity study, as well as an investigation into the impact of probe-misalignment and potential benefits of a smaller probe tip, to further broaden the understanding of the electrical properties of thyroid and parathyroid tissue and how impedance measurement may enhance tissue differentiation in thyroid surgery. Given the non-invasive nature of EIS measurement, this would be advantageous for both the surgeon and the patient, in terms of the potential benefits of the EIS-guided parathyroid detection in reducing the risks of hypoparathyroidism and hypocalcaemia.

SUPPLEMENTARY MATERIALS

Supplementary Materials document provides additional information for the Materials and Methods section, including additional description of the Finite Element modelling

approach (Section I) and a detailed summary on the model parameters (Section II). Additionally, the conductivities and permittivities derived from the lower-scale model simulations are summarised in the Supplementary Dataset.

ACKNOWLEDGMENT

The authors would like to acknowledge Zilico Ltd. (https://zilico.co.uk) for obtaining the funding for the project, Prof. Brian Brown for the expertise in the computational modelling relating to Electrical Impedance Spectroscopy, and the IT Services at The University of Sheffield for the provision of services for High Performance Computing.

REFERENCES

[1] D. R. Chadwick, "Hypocalcaemia and permanent hypoparathyroidism after total/bilateral thyroidectomy in the BAETS Registry," *Gland surgery*, vol. 6, no. Suppl 1, pp. S69–S74, dec 2017. [Online]. Available: https://pubmed.ncbi.nlm.nih.gov/29322024https://www.ncbi.nlm.nih.gov/pmc/articles/PMC5756750/

[2] S. L. Hillary, B. H. Brown, N. J. Brown, and S. P. Balasubramanian, "Use of Electrical Impedance Spectroscopy for Intraoperative Tissue Differentiation During Thyroid and Parathyroid Surgery," *World Journal of Surgery*, 2019. [Online]. Available: https://doi.org/10.1007/s00268-019-05169-7

[3] S. W. Kim, H. S. Lee, and K. D. Lee, "Intraoperative real-time localization of parathyroid gland with near infrared fluorescence imaging," *Gland surgery*, vol. 6, no. 5, pp. 516–524, oct 2017.

[4] Y. Shinden, A. Nakajo, H. Arima, K. Tanoue, M. Hirata, Y. Kijima, K. Maemura, and S. Natsugoe, "Intraoperative Identification of the Parathyroid Gland with a Fluorescence Detection System," *World Journal of Surgery*, vol. 41, no. 6, pp. 1506–1512, jun 2017. [Online]. Available: http://link.springer.com/10.1007/s00268-017-3903-0

[5] P. Mohr, U. Birgersson, C. Berking, C. Henderson, U. Trefzer, L. Kemeny, C. Sunderkötter, T. Dirschka, R. Motley, M. Frohm-Nilsson, U. Reinhold, C. Loquai, R. Braun, F. Nyberg, and J. Paoli, "Electrical impedance spectroscopy as a potential adjunct diagnostic tool for cutaneous melanoma," *Skin Research and Technology*, vol. 19, no. 2, pp. 75–83, may 2013. [Online]. Available: https://doi.org/10.1111/srt.12008

[6] B. H. Brown, J. A. Tidy, K. Boston, A. D. Blackett, R. H. Smallwood, and F. Sharp, "Relation between tissue structure and imposed electrical current flow in cervical neoplasia," *The Lancet*, vol. 355, no. 9207, pp. 892–895, 2000. [Online]. Available: https://www.sciencedirect.com/science/article/pii/S0140673699090959

[7] C. Murdoch, B. H. Brown, V. Hearnden, P. M. Speight, K. D'Apice, A. M. Hegarty, J. A. Tidy, T. J. Healey, P. E. Highfield, and M. H. Thornhill, "Use of electrical impedance spectroscopy to detect malignant and potentially malignant oral lesions," *International journal of nanomedicine*, vol. 9, pp. 4521–4532, sep 2014. [Online]. Available: https://pubmed.ncbi.nlm.nih.gov/25285005https://www.ncbi.nlm.nih.gov/pmc/articles/PMC4181751/

[8] B. A. Wilkinson, R. H. Smallwood, A. Keshtar, J. A. Lee, and F. C. Hamdy, "Electrical Impedance Spectroscopy and the Diagnosis of Bladder Pathology: A Pilot Study," *The Journal of Urology*, vol. 168, no. 4, Part 1, pp. 1563–1567, 2002. [Online]. Available: https://www.sciencedirect.com/science/article/pii/S0022534705645211

[9] V. Mishra, H. Bouayad, A. Schned, J. Heaney, and R. J. Halter, "Electrical impedance spectroscopy for prostate cancer diagnosis," in *2012 Annual International Conference of the IEEE Engineering in Medicine and Biology Society*, 2012, pp. 3258–3261.

[10] A. Stojadinovic, A. Nissan, Z. Gallimidi, S. Lenington, W. Logan, M. Zuley, A. Yeshaya, M. Shimonov, M. Melloul, S. Fields, T. Allweis, R. Ginor, D. Gur, and C. Shriver, "Electrical Impedance Scanning for the Early Detection of Breast Cancer in Young Women: Preliminary Results of a Multicenter Prospective Clinical Trial," *Journal of clinical oncology : official journal of the American Society of Clinical Oncology*, vol. 23, pp. 2703–2715, apr 2005.

[11] C. A. González-Correa, B. H. Brown, R. H. Smallwood, N. Kalia, C. J. Stoddard, T. J. Stephenson, S. J. Haggie, D. N. Slatter, and K. D. Bardhan, "Virtual Biopsies in Barrett's Esophagus Using an Impedance Probe," *Annals of the New York Academy of Sciences*, vol. 873, no. 1, pp. 313–321, apr 1999. [Online]. Available: https://doi.org/10.1111/j.1749-6632.1999.tb09479.x

[12] Zilico Limited, "ZedScan™ a new standard in colposcopy - technical brochure." [Online]. Available: www.zilico,co.uk

[13] D. C. Walker, "Modeling the Electrical Properties of Cervical Epithelium," Ph.D. dissertation, University of Sheffield, 2001.

[14] D. C. Walker, R. H. Smallwood, A. Keshtar, B. A. Wilkinson, F. C. Hamdy, and J. A. Lee, "Modelling the electrical properties of bladder tissuequantifying impedance changes due to inflammation and oedema," *Physiological Measurement*, vol. 26, no. 3, pp. 251–268, 2005.

[15] J. P. Heath, K. D. Hunter, C. Murdoch, and D. C. Walker, "Computational Modelling for Electrical Impedance Spectroscopy-Based Diagnosis of Oral Potential Malignant Disorders (OPMD)," 2022.

[16] A. Hartinger, R. Guardo, V. Kokta, and H. Gagnon, "A 3-D Hybrid Finite Element Model to Characterize the Electrical Behavior of Cutaneous Tissues," *Biomedical Engineering, IEEE Transactions on*, vol. 57, pp. 780–789, may 2010.

[17] U. Birgersson, E. Birgersson, and S. Ollmar, "Estimating electrical properties and the thickness of skin with electrical impedance spectroscopy: Mathematical analysis and measurements," *Journal of Electrical Bioimpedance*, vol. 3, jul 2012.

[18] S. Huclova, D. Erni, and J. Fröhlich, "Modelling effective dielectric properties of materials containing diverse types of biological cells," *Journal of Physics D: Applied Physics*, vol. 43, no. 36, p. 365405, 2010. [Online]. Available: http://dx.doi.org/10.1088/0022-3727/43/36/365405

[19] ——, "Modelling and validation of dielectric properties of human skin in the MHz region focusing on skin layer morphology and material composition," *Journal of Physics D: Applied Physics*, vol. 45, no. 2, p. 025301, jan 2012. [Online]. Available: http://stacks.iop.org/0022-3727/45/i=2/a=025301?key=crossref.48544880ea59acc1fd00f0b22bef3b80

[20] Y. Lv, Y. Zhang, J. Huang, Y. Wang, and B. Rubinsky, "A Study on Nonthermal Irreversible Electroporation of the Thyroid," *Technology in Cancer Research Treatment*, vol. 18, p. 1533033819876307, jan 2019. [Online]. Available: https://doi.org/10.1177/1533033819876307

[21] N. Nasir and M. Al Ahmad, "Cells Electrical Characterization: Dielectric Properties, Mixture, and Modeling Theories," *Journal of Engineering*, vol. 2020, p. 9475490, 2020. [Online]. Available: https://doi.org/10.1155/2020/9475490

[22] M. Al-Zghoul, "Macro- and Micro-Morphological Studies on the Parathyroid Glands of Dromedary Camel," *Pakistan Veterinary Journal*, vol. 37, pp. 59–64, jan 2017.

[23] G. H. Markx, C. L. Davey, and D. B. Kell, "To what extent is the magnitude of the Cole-Cole α of the β-dielectric dispersion of cell suspensions explicable in terms of the cell size distribution?" *Bioelectrochemistry and Bioenergetics*, vol. 25, no. 2, pp. 195–211, 1991. [Online]. Available: https://www.sciencedirect.com/science/article/pii/030245989187003Y

[24] A. Saltelli, K. Aleksankina, W. Becker, P. Fennell, F. Ferretti, N. Holst, S. Li, and Q. Wu, "Why so many published sensitivity analyses are false: A systematic review of sensitivity analysis practices," *Environmental Modelling Software*, vol. 114, pp. 29–39, 2019. [Online]. Available: https://www.sciencedirect.com/science/article/pii/S1364815218302822